Title

Implementation and evaluation of a generalized radiative transfer scheme within canopy in the soil-vegetation-atmosphere transfer (SVAT) model

Journal

Journal of Geophysical Research: Atmospheres, 121(20)

ISSN

2169-897X

Authors

Qiu, Bo
Guo, Weidong
Xue, Yongkang
et al.

Publication Date

2016-10-27

DOI

10.1002/2016jd025328

Peer reviewed

AGU PUBLICATIONS

JGR

Journal of Geophysical Research: Atmospheres

RESEARCH ARTICLE
10.1002/2016JD025328

Key Points:
- A generalized radiative transfer scheme within canopy was implemented
- Nonuniform leaf angle distribution was considered in the areas of broadleaf trees
- Albedo was increased due to nonuniform leaf optical properties in the boreal winter

Correspondence to:
W. Guo and Y. Xue,
guowd@nju.edu.cn;
yxue@geog.ucla.edu

Citation:
Qiu, B., W. Guo, Y. Xue, and Q. Dai (2016), Implementation and evaluation of a generalized radiative transfer scheme within canopy in the soil-vegetation-atmosphere transfer (SVAT) model, *J. Geophys. Res. Atmos.*, *121*, 12,145–12,163, doi:10.1002/2016JD025328.

Received 5 MAY 2016
Accepted 10 OCT 2016
Accepted article online 12 OCT 2016
Published online 28 OCT 2016

Implementation and evaluation of a generalized radiative transfer scheme within canopy in the soil-vegetation-atmosphere transfer (SVAT) model

Bo Qiu[1,2], Weidong Guo[1,3,4], Yongkang Xue[2], and Qiudan Dai[5]

[1]Institute for Climate and Global Change Research, School of Atmospheric Sciences, Nanjing University, Nanjing, China, [2]Department of Geography and Department of Atmospheric and Oceanic Sciences, University of California, Los Angeles, California, USA, [3]Joint International Research Laboratory of Atmospheric and Earth System Sciences of Ministry of Education, Nanjing, China, [4]Collaborative Innovation Center of Climate Change, Jiangsu Province, Nanjing, China, [5]State Key Laboratory of Numerical Modeling for Atmospheric Sciences and Geophysical Fluid Dynamics, Institute of Atmospheric Physics, Chinese Academy of Sciences, Beijing, China

Abstract The process of radiative transfer over vegetated areas has a profound impact on energy, water, and carbon balances over the terrestrial surface. In this paper, a generalized radiative transfer scheme (GRTS) within canopy is implemented in the Simplified Simple Biosphere land surface model (SSiB). The main concept and structure of GRTS and its coupling methodology to a land model are presented. Different from the two-stream method, the GRTS takes into account the effects of complex canopy morphology and inhomogeneous optical properties of leaves on radiative transfer process within the canopy. In the offline SSiB/GRTS simulation for the period of 2001–2012, the nonuniform leaf angle distribution within canopy layers is considered in SSiB/GRTS in the areas of evergreen broadleaf trees. Compared with the SSiB/two stream method, SSiB/GRTS produces lower canopy reflectance and higher transmittance, which leads to more realistic albedo simulation. The canopy-absorbed radiation flux in SSiB/GRTS simulation is lower than that in SSiB/two stream method simulation throughout the year in the areas of evergreen broadleaf trees. The largest difference of $-18.4\ W/m^2$ occurs in the Amazon region in the autumn. The ground-absorbed radiation flux increases in the SSiB/GRTS simulation, especially in the spring and autumn. The largest difference in the ground-absorbed radiation flux between SSiB/GRTS simulation and SSiB/two stream method simulation is $25.45\ W/m^2$. In the boreal winter season, compared with the two-stream method in the SSiB, the GRTS gives higher surface albedo in the areas with high snow cover fraction over leaf.

1. Introduction

The process of radiative transfer within canopy, which includes the reflected and absorbed radiation by canopy and ground, has a profound impact on the distribution of the solar radiation between the surface and the atmosphere. And this issue is essential for land surface modeling [*Sellers*, 1985; *Yuan et al.*, 2014]. Surface albedo, which is important for the surface energy budget and surface-atmosphere interaction, is defined as the ratio of reflected solar radiation to incident solar radiation. The sensitivity of the climate system to surface albedo has been tested in many previous studies [*Charney et al.*, 1977; *Sud and Fennessy*, 1982; *Xue and Shukla*, 1993; *Dirmeyer and Shukla*, 1996], which indicates that the changes in surface albedo have an effect on surface energy and affect latent and sensible heat fluxes, eventually leading to changes in atmospheric circulation and precipitation. The surface albedo plays a key role in climate simulations [*Wang et al.*, 2006; *Gu et al.*, 2002; *Li et al.*, 2015]. Moreover, the visible radiation absorbed by the canopy is one of the critical factors of affecting transpiration, photosynthesis, and carbon exchange between the canopy and the atmosphere. In addition, the radiation absorbed by the ground is a basic control factor in determining the water and energy exchanges between the soil and snow. Therefore, the importance of canopy radiative transfer process has been stressed in the development of biogeophysical and biogeochemical models.

Surface albedos simulated by climate models have been compared with satellite-derived albedos and large differences have been found [*Oleson et al.*, 2003]. The previous climate sensitivity studies have suggested that an albedo error larger than 0.02–0.05 can lead to significant responses in climate models [*Xue et al.*, 2010]. The range of 0.02–0.05 is thus considered to be a constraint for the albedo accuracy requirement. Snow over the canopy makes the albedo simulation more complex. And the snow-masking effect of vegetation has been proved to be a major error source for albedo simulation in climate models. For example, *Loranty et al*. [2014] compared surface albedos from the Coupled Model Intercomparison Project Phase 5 (CMIP5) models with Moderate Resolution Imaging Spectroradiometer (MODIS) products for the Northern Hemisphere and found that the snow-masking effect of the canopy has a profound influence on the surface albedo in the high northern latitudes. *Brovkin et al*. [2013] compared the surface albedos from the Earth system models with MODIS surface albedo observations for the period of 2001 to 2010. The major bias of modeled surface albedo occurs in the winter and spring in high northern latitude ecosystems. The high sensitivity of the albedo to the snow cover simulation in the canopy can attribute to the disagreements between modeled and observed land surface albedos. *Wang et al*. [2006] evaluated the surface albedos from 17 climate models over northern latitudes the Western Hemisphere and found that these climate models overestimate the surface albedos by up to 0.05 in the summer. Furthermore, the winter albedo bias is generally larger than that in the summer.

The two-stream approximation method was applied to the description of radiative transfer in atmospheres [*Meador and Weaver*, 1980]. In early land surface models, this method was introduced to describe radiative transfer process within the canopy [*Dickinson*, 1983; *Sellers*, 1985]. Some simplifications are assumed to derive the equations for the two-stream method: (1) the incident diffuse sky radiation and the scattered radiation in the canopy are isotropic in the upward and downward directions, (2) the structure of the canopy is uniform in the vertical direction, and (3) the adaxial and abaxial leaf surfaces have the same optical properties. Under the above simplifications, a simple but reasonably realistic analytical approach was developed to obtain land surface albedo efficiently. The two-stream approximation method was widely applied to describe radiative transfer process within canopy in current land surface models [*Sellers et al*., 1986, 1996; *Dickinson et al*., 1986; *Liang*, 2004; *Dai and Zeng*, 1997; *Niu et al*., 2011].

However, the two-stream method cannot accurately describe the realistic radiative transfer process within canopy due to the unrealistic assumptions in simplifying the governing equations. For example, the optical properties of the adaxial and abaxial leaf surfaces are the same in the two-stream method, but in reality, the difference is notable based on measurements. The adaxial and abaxial aspen and hazelnut leaf reflectances were measured in the Boreas Project in the U.S., and the differences in optical properties are notable [*Mesarch et al*., 1998]. Furthermore, the reflectance of the adaxial leaf surface would increase greatly when snow covers the leaf surface, but the reflectance of the abaxial surface would change little. Thus, snow cover makes a great difference in the optical properties of adaxial and abaxial leaf surfaces. This kind of difference should be considered in the radiative transfer model.

To overcome the shortcoming in the two-stream method, *Tian et al*. [2007] developed an analytical four-stream approximation method. The equations were derived by the approximation of four isotropic intensities in a homogeneous canopy. The modeled albedo, transmittance, and absorptance became better in the four-stream approximation method than that in the two-stream method. But this scheme still assumes the same optical properties of the adaxial and abaxial leaf surfaces and a uniform vertical canopy structure. In addition, the concepts of clumping index and gap probability were introduced into the radiative transfer model. *Yang et al*. [2001] and *Wang et al*. [2007] took into account the 3-D geometry of canopy to modify the two-stream method. These models have improved albedo simulation, but they are highly dependent on correct estimates of clumping indices or gap probability under different conditions. Recently, *Yuan et al*. [2014] developed a new framework of canopy radiative transfer model based on the 3-D structural canopy effects. The simulations of this new model have shown good agreements with observations in several case studies. To derive the analytical solution, however, some simple and ideal canopy structures have to be specified.

In this study, we have applied a layered radiative transfer scheme [*Dai and Sun*, 2006] based on previous studies [*Goudriaan*, 1977; *Norman and Jarvis's*, 1975] to simulate the physical process of radiative transfer in the canopy. This is a more general layered radiative transfer scheme, which is referred to as the generalized radiative transfer scheme (GRTS). This new scheme can deal with radiative transfer process within the canopy, which has nonuniform leaf optical properties and vertical structure. The GRTS had been compared to two-stream method in some ideal experiments [*Dai and Sun*, 2006, 2007], but it has not been implemented in the soil-vegetation-atmosphere-transfer (SVAT) models and evaluated using observed albedo data. We couple the GRTS with the Simplified Simple Biosphere (SSiB) land surface model [*Xue et al*., 1991, 1996a, 2003; *Zhan et al*., 2003] and evaluate its performance in simulating the surface albedo and the absorption of radiation by canopy and ground. SSiB is a biophysically based model that provides estimates of surface albedo for

Table 1. List of Symbols With Definition

Symbol	Definition
β	inclination angle of incident diffuse radiation
β_0	inclination angle of the direct sunbeam
β'	the inclination angle of scattered diffuse radiation
I_0	the beam flux at the canopy top
L	accumulated leaf area index from the canopy top
$\tilde{I}(\beta', L)$	the diffuse radiation flux
ω	leaf scattering coefficient
$P(\beta', \beta)$	normalized scattering phase function of the radiation
μ	$\mu = \sin\beta$
μ_0	$\mu_0 = \sin\beta_0$
$\overline{G}$	mean geometric function

direct and diffuse radiation at visible and near-infrared, surface radiation fluxes, momentum, sensible heat, latent heat, and carbon, as well as runoff, soil moisture, and ice content, snow water equivalent, surface temperatures, net primary productivity, and other variables relevant to surface water, carbon, and energy balances [*Xue et al.*, 1991; *Sun and Xue*, 2001; *Li et al.*, 2010]. The two-stream method is used to describe the radiative transfer with canopy. An analytical solution was developed and incorporated to SSiB2 [*Zhan et al.*, 2003]. And the SSiB has been validated and evaluated by a lot of observational data from different sites and vegetation types [e.g., *Xue et al.*, 1996b, 2003] and widely used in global and regional climate studies [e.g., *Xue et al.*, 2010; *Chou et al.*, 2002]. Two main goals of this study are (1) to examine the importance of nonuniform leaf angle distribution in the broadleaf evergreen trees areas and (2) to examine the importance of nonuniform leaf optical properties in the boreal winter. The results are compared with those from the two-stream method and verified against observational data. Possible reasons for the differences are analyzed. This paper is organized as follows. A brief description of the GRTS is given in section 2. Section 3 describes the MODIS surface albedo data sets, which are used for the model evaluation. Section 4 describes the evaluation and comparison of simulated surface albedo using the two radiative transfer schemes. Discussion and conclusions are presented in section 5.

2. Model Descriptions

2.1. General Expression for the Canopy Radiative Transfer Equation

The theory for radiative transfer scheme within the canopy developed previously and the derivation of the canopy radiative transfer equation is very complicated [*Myneni et al.*, 1988]. The final expression of the generalized radiation transfer equation in the canopy that presented in these previous studies is written as

$$-\mu\frac{\partial\tilde{I}(\beta',L)}{\partial L}+\overline{G}(\beta')\tilde{I}(\beta',L)=\frac{\omega}{2}\int_{-1}^{1}\tilde{I}(\beta,L)\overline{G}(\beta)P(\beta',\beta)d\beta$$
$$+\frac{\omega}{4}P(\beta',\beta_0)\overline{G}(\beta_0)I_0 exp\left(\frac{-G(\beta_0)L}{\mu_0}\right). \quad (1)$$

In equation (1), the first term on the left side describes the attenuation of diffuse radiation $\tilde{I}(\beta', L)$ within the canopy, the second term describes the loss of diffuse radiation $\tilde{I}(\beta', L)$ that is intercepted by leaves, and geometric function $\overline{G}(\beta')$ is the relative projection area of leaf elements in the direction β'. The first term on the right side describes the contribution of the diffuse light in the direction β' coming from all directions to $\tilde{I}(\beta', L)$, and the second term on the right side refers to the contribution to $\tilde{I}(\beta', L)$ by the scattering of direct incident flux. Table 1 lists symbols with definition.

2.2. General Structure of the GRTS

In the GRTS, the canopy is assumed to be horizontally infinite, continuous, and uniform in this new radiative transfer scheme. And this scheme is required to have no horizontal interaction within one single layer. Thus, the GRTS is a layered radiative transfer scheme, and the canopy is divided into several layers vertically. For the convenience, the order number of each layer is assigned from top layers to bottom layers. For example, for the top layer, $j = 1$, and for the soil surface, $j = M$. The schematic diagram of the scheme structure is shown in Figure 1. In each layer, the leaf area index (LAI) should be very small to avoid mutual shading interaction and multiple scattering. Thus, $dL_j \leq 0.1$ is used in this paper [*Goudriaan*, 1977].

In order to have a better understanding of the derivation, some notations are defined as follows. β_k ($k = 1, 2, 3, \ldots, 9$) is the incident inclination angle of diffuse radiation; β_n' ($n = 1, 2, 3, \ldots, 9$) is the inclination angle of the

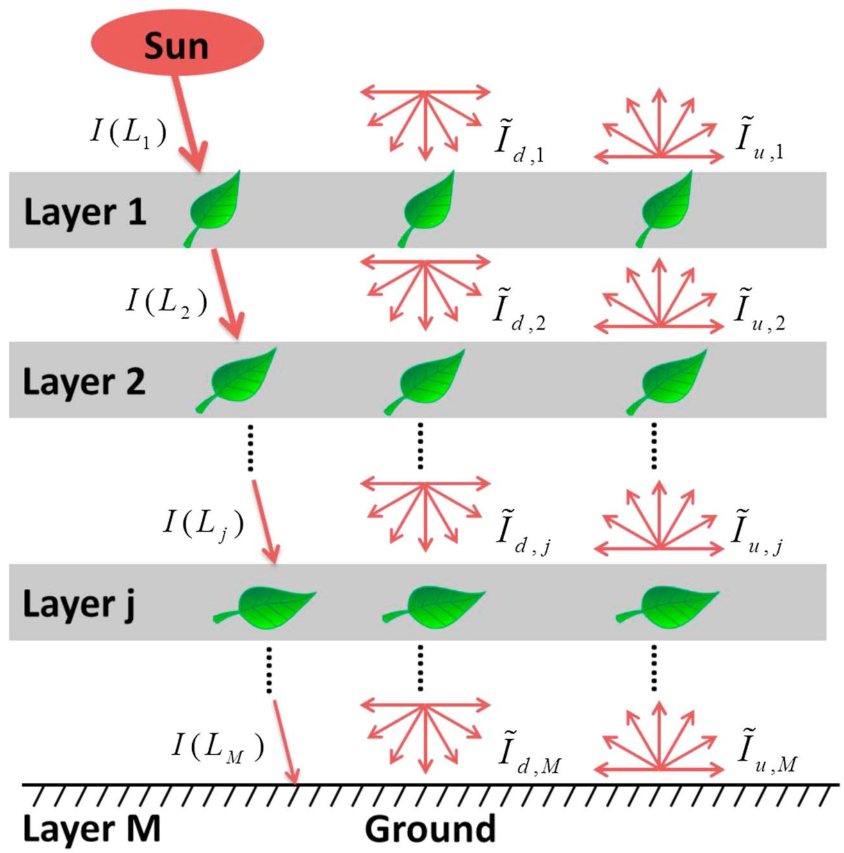

Figure 1. Schematic diagram of the generalized layered radiative transfer model.

scattered radiation which is intercepted by the leaves; θ is the leaf inclination angle; β_k, β_n', and θ are shown in Figure 2. $\tilde{I}_d(\beta_k, j)$ and $\tilde{I}_u(\beta_k, j)$ are the downward and upward diffuse radiation between layers $j-1$ and j, respectively. And they are functions of incident inclination angle β_k.

2.3. General Expression for Geometric Function and Scattering Distribution Function

Geometric function describes the effective portion of the unit leaf area to intercept the light and the derivation of the function in GRTS can be found in the paper of *Dai and Sun* [2006]. The leaf angle distribution function $g(\theta)$ is a mathematical description of the probability density function of angular orientation of the leaves in the vegetation. When $g(\theta)$ is given, the mean geometric function $\overline{G}(\beta_k, \theta)$ can be written as

$$\overline{G}(\beta_k, \theta) = \sum_{n=1}^{9} g_n(\theta) G(\beta_k, \theta). \quad (2)$$

Therefore, for the leaves with a specific inclination θ in layer j, the intercepted fraction is proportional to the average projection and inversely proportional to the sine of the inclination of the incident light; thus, it is written as

$$M_i(\beta_k, \theta) = dL_j \overline{G}(\beta_k, \theta)/\sin\beta_k. \quad (3)$$

The nonintercepted radiation is

$$M_t(\beta_k, \theta) = 1 - M_i(\beta_k, \theta) \quad (4)$$

In GRTS, according to the previous studies [*Goudriaan*, 1977; *Wohlfahrt et al.*, 2000], the expression of anisotropic scattering distribution function $B_l(\beta_n', \theta)$ is

$$B_l(\beta_n', \theta) = \frac{B_u(\beta_n') M_i(\beta_n', \theta)}{\sum_{k=1}^{9} B_u(\beta_k) M_i(\beta_k, \theta)}. \quad (5)$$

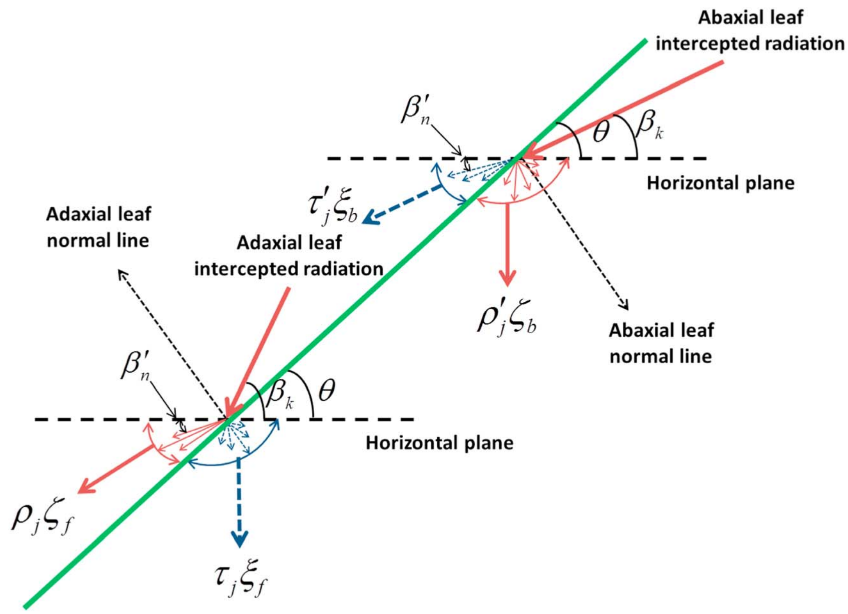

Figure 2. Schematic diagram of the downward light diffusion at specific incident inclination angles at abaxial and adaxial leaf surfaces.

B_u is sky diffuse distribution function with the inclination angle $\beta_n^{'}$. The diffuse radiation within the canopy is composed of two parts: (1) the sky diffuse radiation and (2) the direct beam radiation intercepted by the canopy. For the sky diffuse radiation, the intensity is generally defined by a distribution in several subsectors in the inclined direction. According to nine subsectors used in *Dai and Sun* [2006], B_u is given as

$$B_u(n = 1, 2, 3, \ldots, 9) = (0.030, 0.087, 0.133, 0.163, 0.174, 0.163, 0.133, 0.087, 0.030).$$

2.4. Numerical Solution

In GRTS, for layer j, the adaxial leaf reflectance and transmittance are presented as ρ_j and τ_j and the abaxial leaf reflectance and transmittance are presented as $\rho_j^{'}$ and $\tau_j^{'}$. The basic equation of the downward radiation is

$$\widetilde{I}_d(j+1) = \widetilde{I}_{d,\,\text{nonintercepted}} + \widetilde{I}_{d,\,\text{intercepted}} + I_{d,\,\text{sunbeam}}. \tag{6}$$

The downward radiation $\tilde{I}_d(j+1)$ is composed of three parts. The first part is the radiation contributed by the nonintercepted part of $\widetilde{I}_d\left(\beta_n^{'}, j\right)$. The second part includes the radiation contributed by scattering the intercepted part of $\tilde{I}_d(\beta_k, j)$ and $\tilde{I}_u(\beta_k, j+1)$. The third part is the radiation contributed by the sunbeam.

1. $\widetilde{I}_{d,\,\text{nonintercepted}}$

The fraction of nonintercepted radiation through the layer of each leaf angle is $g_j(\lambda)M_t\left(\beta_n^{'}, \lambda\right)$, so the total 9 angle is

$$\widetilde{I}_{d,\,\text{nonintercepted}} = \sum_{n=1}^{9} g_j(\theta)M_t\left(\beta_n^{'}, \theta\right)\widetilde{I}_d\left(\beta_n^{'}, j\right). \tag{7}$$

2. $\widetilde{I}_{d,\,\text{intercepted}}$

$\tilde{I}_{d,\text{intercepted}}$ is composed of the contribution of $\tilde{I}_d(\beta_k, j)$ and $\tilde{I}_u(\beta_k, j+1)$. The fraction of intercepted radiation penetrating through the layer of each leaf angle is $g_j(\theta)B_l\left(\beta_n^{'}, \theta\right)$, and each incident inclination angle is M_i (β_k, θ). A downward radiation intercepted by layer j will be scattered (both reflected and transmitted) in all directions and contribute to $\widetilde{I}_d\left(\beta_n^{'}, j+1\right)$. Figure 2 shows schematic diagram of the downward light diffusion at specific leaf angle and incident inclination angle at abaxial and adaxial leaf surfaces. The leaf surface is considered as a Lambertian scatterer, for diffuse radiation incident from above, the intercepted radiation scattering is composed of four parts. $\rho_j\zeta_f$ and $\rho_j^{'}\zeta_b$ are the radiation reflected by the adaxial and the abaxial leaf surface, respectively. $\tau_j\xi_f$ and $\tau_j^{'}\xi_b$ are the radiation transmitted through the adaxial and abaxial leaf surface, respectively. ξ_f, ξ_b, ζ_f, and ζ_b are the ratios of the four parts to the total scattered contribution of $\tilde{I}_d(\beta_k, j)$ to $\tilde{I}_d\left(\beta_n^{'}, j+1\right)$. They are functions of $\beta_n^{'}$, β_k, and θ: $\xi_f = \xi_f\left(\beta_k, \beta_n^{'}, \theta\right)$, $\xi_b = \xi_b\left(\beta_k, \beta_n^{'}, \theta\right)$, $\zeta_f = \zeta_f\left(\beta_k, \beta_n^{'}, \theta\right)$, and $\zeta_b = \zeta_b\left(\beta_k, \beta_n^{'}, \lambda\right)$. The optical geometry method is used to calculate the ratio of each part. The detailed derivation of this method can be found in the *Dai and Sun* [2006]. The contribution by scattering the intercepted fraction of $\tilde{I}_d(\beta_k, j)$ is

$$\sum_{n=1}^{9}\left[g_j(\theta)B_l\left(\beta_n^{'},\theta\right)\sum_{k=1}^{9}M_i(\beta_k,\theta)\tilde{I}_d(\beta_k,j)\left(\rho_j\zeta_f+\rho_j^{'}\zeta_b+\tau_j\xi_f+\tau_j^{'}\xi_b\right)\right]. \quad (8)$$

The contribution by scattering the intercepted fraction of $\tilde{I}_u(\beta_k, j+1)$ is very similar to $\tilde{I}_d(\beta_k, j)$, and $\tilde{I}_{d,\text{intercepted}}$ is

$$\tilde{I}_{d,\,\text{intercepted}} = \sum_{n=1}^{9}\left[g_j(\theta)B_l\left(\beta_n^{'},\theta\right)\sum_{k=1}^{9}M_i(\beta_k,\theta)(\text{frac1}_d+\text{frac2}_d)\right], \quad (9)$$

$$\text{frac1}_d = \tilde{I}_d(\beta_k,j)\left(\rho_j\zeta_f+\rho_j^{'}\zeta_b+\tau_j\xi_f+\tau_j^{'}\xi_b\right), \quad (10)$$

$$\text{frac2}_d = \tilde{I}_u(\beta_k,j+1)\left(\rho_j\xi_b+\rho_j^{'}\xi_f+\tau_j\zeta_b+\tau_j^{'}\zeta_f\right). \quad (11)$$

3. $I_{d,\,\text{sunbeam}}$

The penetrating part of the direct beam is transferred continuously downward in its original direction. And the intercepted direct beam turns into diffuse radiation and scatters in all directions. The attenuation of the direct beam within the canopy obeys Beer's law as follows:

$$I(L_j) = I(L_1)e^{-L_{j-1}\frac{\overline{G}_j(\beta_0,\theta)}{\sin\beta_0}}, \quad (12)$$

where $I(L_1)$ is the direct beam at the top of the canopy, $I(L_j)$ is the direct beam at layer j with accumulated leaf area L_{j-1}, and $\frac{\overline{G}_j(\beta_0,\theta)}{\sin\beta_0}$ is the extinction coefficient of the direct beam.

The fraction of intercepted direct beam through the layer of each leaf angle is $g(\theta)B_l\left(\beta_n^{'},\theta\right)$, and the contribution fraction of intercepted direct beam of each layer is

$$\left(\rho_j\zeta_{f,B}+\rho_j^{'}\zeta_{b,B}+\tau_j\xi_{f,B}+\tau_j^{'}\xi_{b,B}\right). \quad (13)$$

$\xi_{f,B}$, $\xi_{b,B}$, $\zeta_{f,B}$, and $\zeta_{b,B}$ are the same functions as ξ_f, ξ_b, ζ_f, and ζ_b, but they use beam inclination angle β_0 instead of β_k. The subscript B refers to direct beam. So $\xi_{f,B} = \xi_{f,B}\left(\beta_0, \beta_n^{'}, \theta\right)$, $\xi_{b,B} = \xi_{b,B}\left(\beta_0, \beta_n^{'}, \theta\right)$, $\zeta_{f,B} = \zeta_{f,B}\left(\beta_0, \beta_n^{'}, \theta\right)$, and $\zeta_{b,B} = \zeta_{b,B}\left(\beta_0, \beta_n^{'}, \theta\right)$.

The contribution of sunbeam is

$$I_{d,\,\text{sunbeam}} = \sum_{n=1}^{9}\left[g_j(\theta)B_l\left(\beta_n^{'},\theta\right)I_B(z=L_j)\cdot dL_j\cdot\frac{\overline{G}_j(\beta_0,\theta)}{\sin\beta_0}\left(\rho_j\zeta_{f,B}+\rho_j^{'}\zeta_{b,B}+\tau_j\xi_{f,B}+\tau_j^{'}\xi_{b,B}\right)\right]. \quad (14)$$

The basic equation of the downward radiation is

$$\tilde{I}_d(j+1) = \tilde{I}_{d,\,\text{nonintercepted}}+\tilde{I}_{d,\,\text{intercepted}}+I_{d,\,\text{sunbeam}}, \quad (15)$$

$$\tilde{I}_{d,\,\text{nonintercepted}} = \sum_{n=1}^{9}g_j(\theta)M_t\left(\beta_n^{'},\theta\right)\tilde{I}_d\left(\beta_n^{'},j\right), \quad (16)$$

$$I_{d,\,\text{sunbeam}} = \sum_{n=1}^{9}\left[g_j(\theta)B_l\left(\beta_n^{'},\theta\right)I_B(z=L_j)\cdot dL_j\cdot\frac{\overline{G}_j(\beta_0,\theta)}{\sin\beta_0}\left(\rho_j\zeta_{f,B}+\rho_j^{'}\zeta_{b,B}+\tau_j\xi_{f,B}+\tau_j^{'}\xi_{b,B}\right)\right], \quad (17)$$

$$\tilde{I}_{d,\,\text{intercepted}} = \sum_{n=1}^{9}\left[g_j(\theta)B_l\left(\beta_n^{'},\theta\right)\sum_{k=1}^{9}M_i(\beta_k,\theta)(\text{frac1}_d+\text{frac2}_d)\right], \quad (18)$$

$$\text{frac1}_d = \tilde{I}_d(\beta_k,j)\left(\rho_j\zeta_f+\rho_j^{'}\zeta_b+\tau_j\xi_f+\tau_j^{'}\xi_b\right), \quad (19)$$

$$\text{frac2}_d = \tilde{I}_u(\beta_k,j+1)\left(\rho_j\xi_b+\rho_j^{'}\xi_f+\tau_j\zeta_b+\tau_j^{'}\zeta_f\right). \quad (20)$$

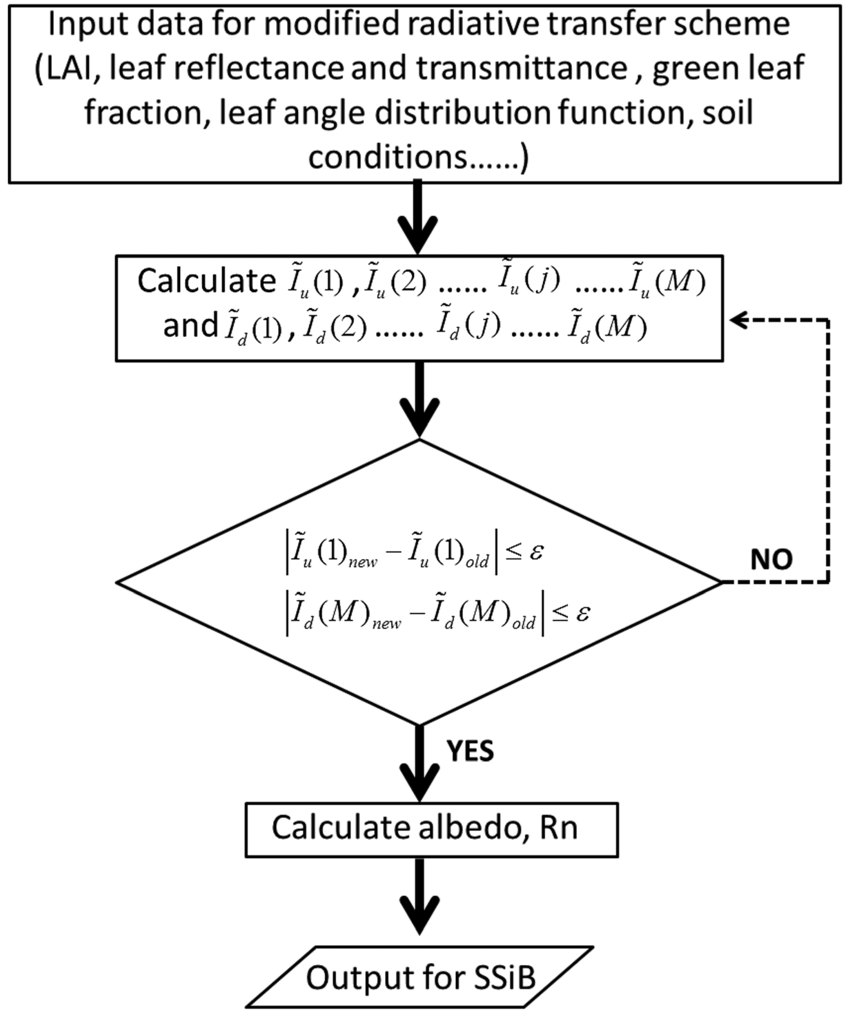

Figure 3. Flow chart of the GRTS coupling to SSiB.

Similarly, the basic equation of the upward radiation is

$$\tilde{I}_u(j) = \tilde{I}_{u,\,\text{nonintercepted}} + \tilde{I}_{u,\,\text{intercepted}} + I_{u,\,\text{sunbeam}}, \tag{21}$$

$$\tilde{I}_{u,\,\text{nonintercepted}} = \sum_{n=1}^{9} g_j(\theta) M_t(\beta_n', \theta) \tilde{I}_u(\beta_n', j+1), \tag{22}$$

$$I_{u,\,\text{sunbeam}} = \sum_{n=1}^{9} \left[g_j(\theta) B_l(\beta_n', \theta) I_B(z = L_j) \cdot dL_j \cdot \frac{\overline{G}_j(\beta_0, \theta)}{\sin\beta_0} \left(\rho_j \xi_{f,B}' + \rho_j' \xi_{b,B}' + \tau_j \zeta_{f,B}' + \tau_j' \zeta_{b,B}' \right) \right], \tag{23}$$

$$\tilde{I}_{u,\,\text{intercepted}} = \sum_{n=1}^{9} \left[g_j(\theta) B_l(\beta_n', \theta) \sum_{k=1}^{9} M_i(\beta_k, \theta) (\text{frac1}_u + \text{frac2}_u) \right], \tag{24}$$

$$\text{frac1}_u = \tilde{I}_d(\beta_k, j) \left(\rho_j \xi_f' + \rho_j' \xi_b' + \tau_j \zeta_f' + \tau_j' \zeta_b' \right), \tag{25}$$

$$\text{frac2}_u = \tilde{I}_u(\beta_k, j+1) \left(\rho_j \xi_f' + \rho_j' \xi_d' + \tau_j \zeta_f' + \tau_j' \zeta_d' \right). \tag{26}$$

Figure 3 is a flow chart of the GRTS coupling to SSiB. This flow chart starts from the SSiB vegetation input data for GRTS. Then the new value of canopy reflectance and transmittance can be obtained by an analytical solution in GRTS. If the value is not close to its previous value, then the canopy reflectance and transmittance can be recomputed. When the value is close to its previous value, the albedo, net radiation (Rn) can be obtained.

Table 2. Designed Experiments With Various Combinations of LAI and Soil Reflectance

Case	LAI	Soil Reflectance
Case 1	0.5	0.1
Case 2	0.5	0.5
Case 3	0.5	0.8
Case 4	1.0	0.1
Case 5	1.0	0.5
Case 6	1.0	0.8
Case 7	3.0	0.1
Case 8	3.0	0.5
Case 9	3.0	0.8
Case 10	5.0	0.1
Case 11	5.0	0.5
Case 12	5.0	0.8

3. Data and Method

3.1. MODIS Albedo Data

MODIS albedo products are used in this study. Currently, the data products are available at 500 m resolution in the sinusoidal projection and 0.05° in the latitude/longitude projection for every 8 days since early 2000 [*Schaaf et al.*, 2002; *Gao et al.*, 2005]. The MCD43C product is used in this study and provides both black-sky albedo (BSA) and white-sky albedo (WSA). MODIS albedo products have been extensively used as a benchmark for evaluating other satellite data and albedo simulations from climate models [*Wang et al.*, 2004; *Stroeve et al.*, 2005; *Cescatti et al.*, 2012; *He et al.*, 2012, 2014].

BSA is a function of solar zenith angle, and it is defined as the albedo without the diffuse radiation component. WSA is independent of solar zenith angle, and it is defined as the albedo without the direct radiation component. The all sky albedo is calculated combining BSA and WSA [*Lucht et al.*, 2000]:

$$\alpha = (1 - f_{dif})\alpha_{bs} + f_{dif}\alpha_{ws}, \tag{27}$$

where α is the all sky albedo, f_{dif} is the diffuse skylight fraction, and α_{bs} and α_{ws} are the BSA and WSA, respectively.

In previous papers, the diffuse skylight fraction has not been taken into consideration when calculating the all-sky albedo [*Zhang et al.*, 2010]. *He et al.* [2014], however, used the monthly diffuse and direct downward radiation from the National Centers for Environmental Prediction (NCEP) reanalysis to calculate the diffuse skylight fraction [*Kalnay et al.*, 1996] and found that the diffuse skylight fraction varies over both time and space. In this study, we use monthly diffuse and direct downward radiation data from NCEP to calculate the diffuse skylight fraction.

3.2. Flux Observation Station and Data

The flux observation data are collected at Semiarid Climate Observatory and Laboratory (SACOL, 104.08°E, 35.57°N), which is one of the reference sites in the Coordinated Energy and Water Cycle Observation Project [*Huang et al.*, 2008]. This site is located at Yuzhong campus of Lanzhou University in Gansu province, which is a typical semiarid region of northwest China. The surface is mainly covered by short grass. The measurements of boundary layer meteorological parameters, surface radiation, surface flux, soil heat, and water moisture are used for evaluation in this study.

4. Sensitivity Studies

4.1. Comparison of Results Between the Two-Stream Method and GRTS With the Nonuniform Leaf Optical Properties

We design two sets of numerical experiments using the GRTS and the two-stream method to assess possible errors and uncertainty of the two methods: one tests the effect for visible radiation (referred to as Exp. VIS) and the other is for near-infrared radiation effect (referred to as Exp. NIR). For simplicity's sake, in all these experiments, transmittance is assigned to be 0.1. For the two-stream method, the leaf reflectance is assigned to be 0.07 and 0.5 in Exp. VIS and Exp. NIR, respectively. But for the GRTS, in Exp. VIS, the adaxial and abaxial leaf reflectances are $\rho = 0.11$ and $\rho' = 0.07$ and in Exp. NIR $\rho = 0.5$ and $\rho' = 0.3$. And the Sun zenith angle is 30° in the two experiments. The different leaf area indices and soil reflectances assigned in the two experiments representing different vegetation and soil conditions. Details regarding the combinations of different LAIs and soil reflectances are listed in Table 2.

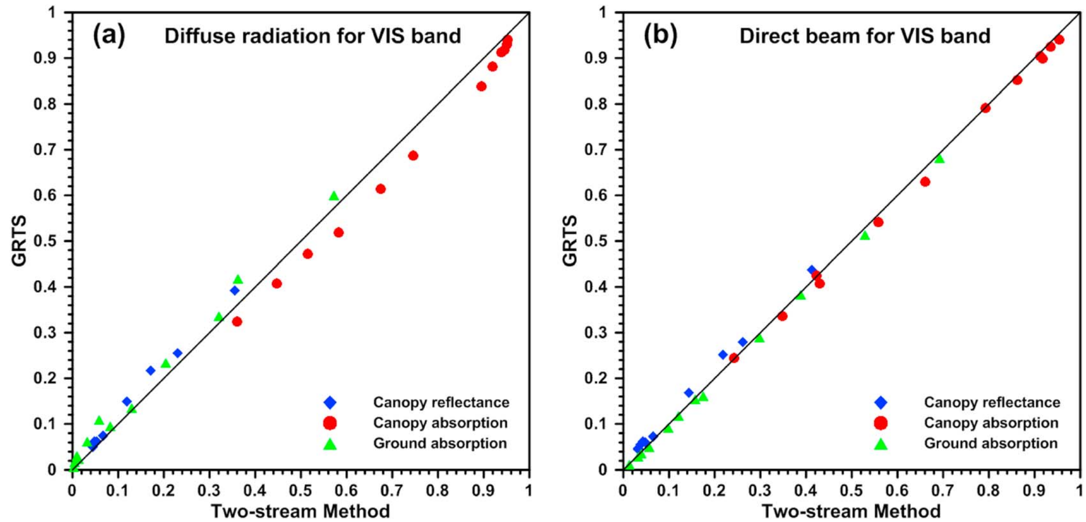

Figure 4. Comparisons of canopy reflectance (blue), canopy absorption (red) and ground absorption (green) between the generalized radiative transfer model and two-stream method for the VIS band: (a) diffuse radiation and (b) direct beam.

Figure 4 shows the comparison of canopy reflectance, canopy absorption, and ground absorption calculated by GRTS and the two-stream method for VIS band. In the VIS band, differences in canopy reflectance and absorption between the GRTS and the two-stream method for diffuse radiation are larger than that for direct beam. The maximum difference in the canopy reflectance is 0.05 with diffuse radiation and 0.03 with direct beam. The maximum difference in the canopy absorption is 0.06 with diffuse radiation and 0.03 with direct beam. The difference in the ground absorption is smaller than that in canopy reflectance and absorption.

Figure 5 shows the comparison of canopy reflectance, canopy absorption, and ground absorption by the GRTS and the two-stream method for NIR band. In the NIR band, the maximum difference in the direct beam is 0.06 with canopy reflectance, 0.05 with canopy absorption, and 0.05 with ground absorption, respectively. Differences in canopy reflectance, canopy absorption, and ground absorption for diffuse radiation are small.

4.2. Comparison of Results Between Uniform and Nonuniform Leaf Angle Distributions

The canopy has a very complicated morphology, and the canopy structure is not uniform in the vertical direction generally. The leaf angle distribution may be different at different canopy heights, especially in the forest

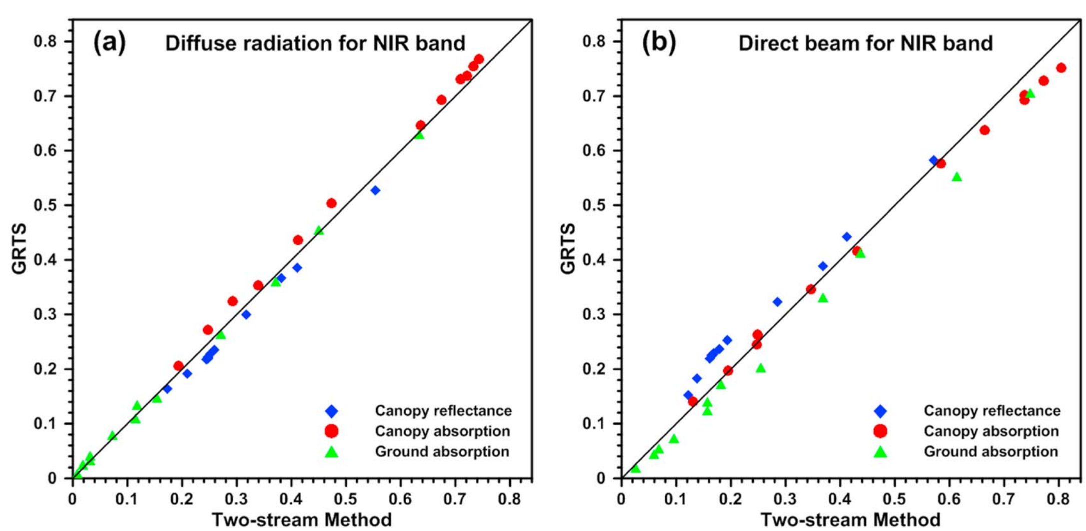

Figure 5. Same as Figure 4 but for the NIR band.

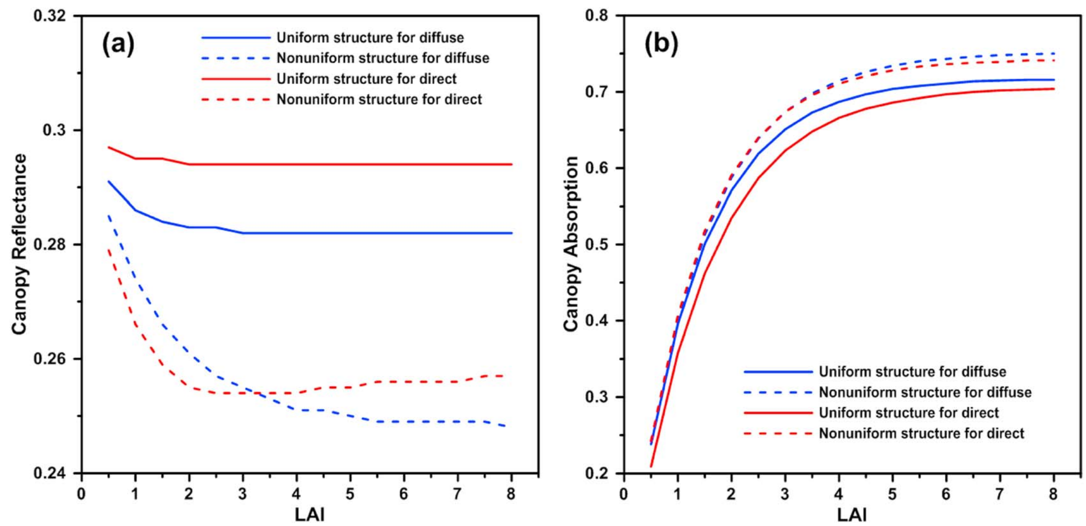

Figure 6. The (a) canopy reflectance and (b) canopy absorption with the uniform and nonuniform leaf inclination angle for the NIR band.

regions. *Jiang* [1996] measured a forest canopy and found that the forest canopy has various leaf angle distributions (LAD) in the vertical direction. The lower layers mostly have planophile LAD; this is caused by the weak light in the lower canopy, and more transmitted radiation can be captured by the horizontal and extended leaves. The upper layers have plagiophile LAD, and this helps more radiation transmitted to the lower layers. The leaf angles in the middle layers are distributed between planophiles and plagiophiles (Figure 1). The measurement of leaf angles of deciduous plants in east Tennessee of the U.S. also showed the similar results. The average leaf angle is about 33° in the entire canopy. But the average leaf angles are 38° in the upper canopy layer, 20° in the middle, and 10° in the lower layer [*Wang and Wang*, 1999]. Hence, in the radiative transfer scheme, the nonuniform canopy structure should be taken into consideration for the forest areas. The MODIS Vegetation Continuous Fields (VCF) products are available at 500 m resolution and provide fractions of three cover types, including trees, herbaceous, and bare ground. Based on the VCF data set, *Yuan et al.* [2014] found that at a single grid, it is rare that only one type of vegetation has a high-percentage cover even within high-resolution grid. Coexisting vegetation covers are widely presented at each grid point.

The GRTS can deal with different leaf angles or multiple layers within a canopy. In order to evaluate possible errors due to a uniform LAD, several sensitivity studies using GRTS are conducted. We use the NIR band and visible band to explore the difference between the uniform and nonuniform LAD. For the NIR band, leaf transmittance is 0.1 and the adaxial and abaxial reflectances are 0.5 and 0.3. For the VIS band, leaf transmittance is 0.1 and the adaxial and abaxial reflectances are 0.11 and 0.07, the same as in previous experiments. The average leaf angles are 30° for the uniform LAD. The leaf angles are 50° at the upper layer and 10° at the lower layer for the nonuniform LAD structure. We compare the results under the two conditions by GRTS with spherical leaves under diffuse radiation and direct beam with the LAI varying from 0.5 to 8.

Figure 6 shows differences in canopy reflectance between these two LADs for NIR band. The difference for high LAIs is larger than that for low LAIs. The biggest difference for diffuse radiation is 0.03 and 0.04 for direct beam. The results for canopy absorption are similar to that for canopy reflectance, and the largest difference is 0.04 for diffuse radiation and 0.06 for direct beam. The differences in ground absorption are small (not shown). Differences in canopy reflectance between these two LADs for the VIS band (Figure 7) show similar results. From Figures 6 and 7, we can see that the uniform LAD has higher canopy reflectance than the nonuniform LAD. To investigate the canopy reflectance difference between these two LADs, we calculate the geometric function for direct beam in these two cases. The value is 0.81 for uniform LAD and 0.76 for nonuniform LAD. The higher value of geometric function means that there will have more intercepted light, which can lead a higher canopy reflectance and a lower transmittance. This result indicates that the application of the two-stream method to a canopy with uniform structure will introduce nonnegligible errors. Moreover, the GRTS is a layered scheme, and LAI in each layer is less than 0.1, which can avoid the effect

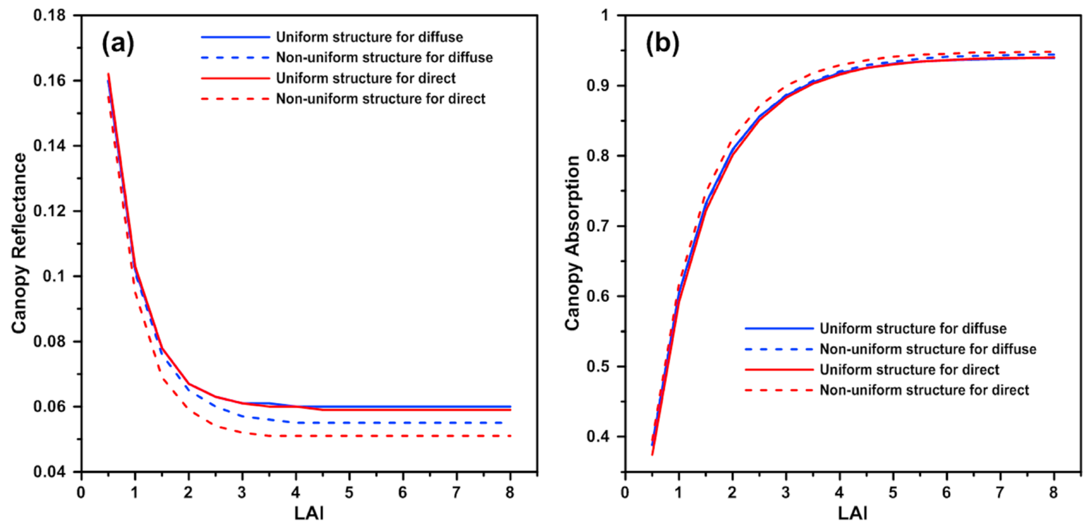

Figure 7. Same as Figure 6 but for the VIS band.

of mutual interactions within the same layer according to the work of *Goudriaan* [1977]. If we increase the LAI of each layer in the cases with high LAI, the canopy reflectance will increase (figure is not shown). This may be caused by the mutual shading interactions between each layer. But in the two-stream method, the canopy is assumed to be one layer. Thereby, GRTS will be more realistic than the two-stream scheme, especially for the regions with high LAIs.

5. Model Evaluation

5.1. Flux Observation Evaluation

The meteorological measurements at half-hour intervals data from SACOL is use as the forcing data for the single point SSiB2 model. The control SACOL run is conducted using the two-stream method, and the sensitivity run using the GRTS is referred to as the GRTS SACOL run. Both experiments cover the period from 2009 to 2010. The first year is taken as a spin-up time, and the results of second year are analyzed below. The upward and downward, shortwave and longwave radiation are measured in this site. And the monthly average albedo is calculated as the ratio between the upward and downward shortwave radiation.

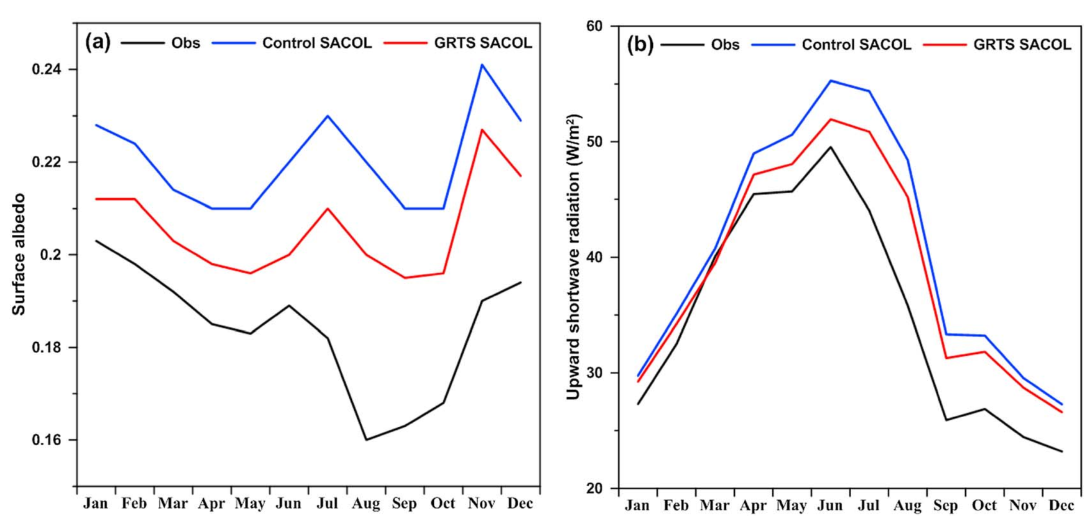

Figure 8. The (a) monthly mean surface albedo and (b) upward shortwave radiation in the observation, control run, and GRTS run in 2010.

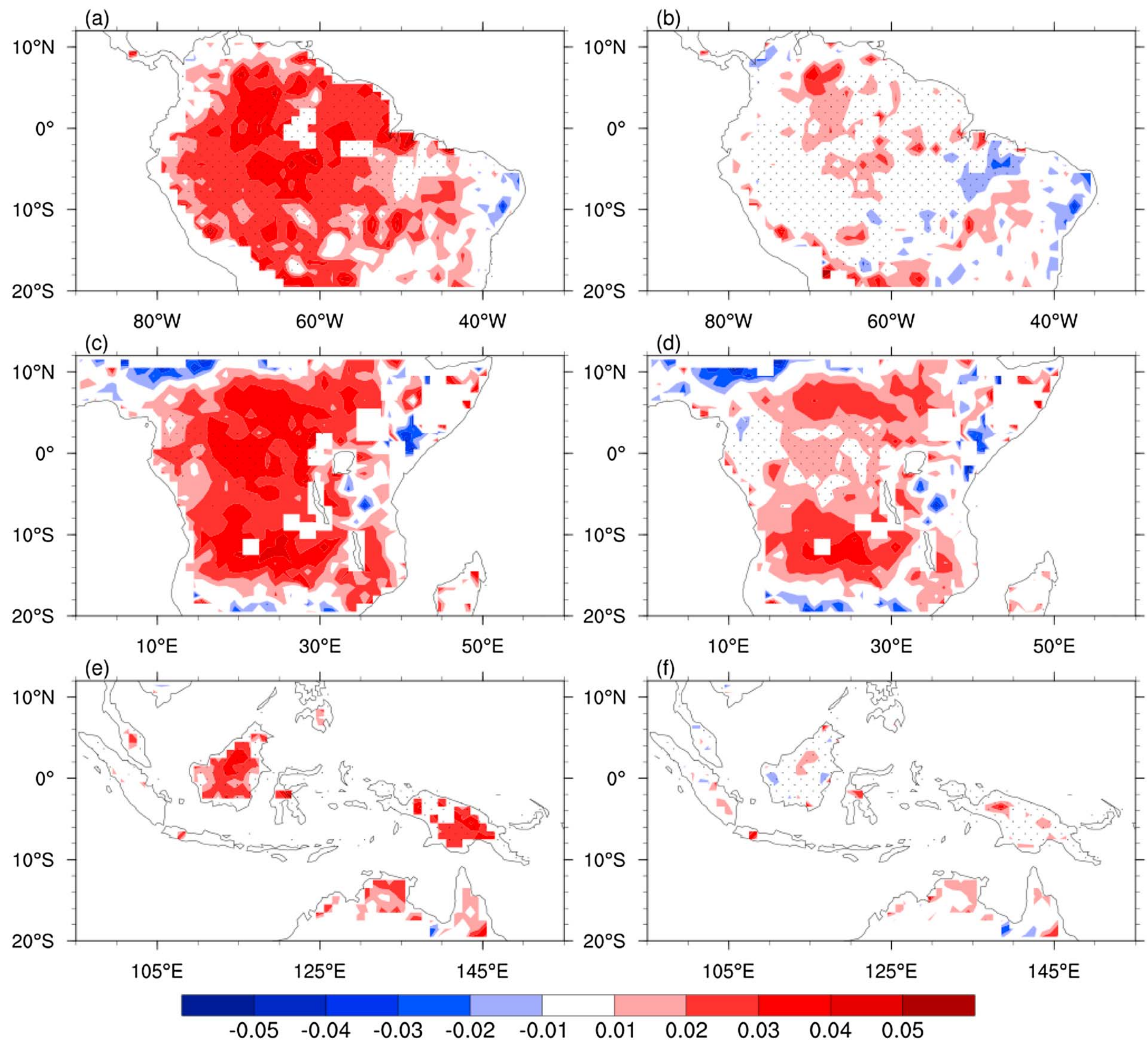

Figure 9. Annual mean error of land surface albedo in simulations of control run (left) and GRTS run (right): (a, b) Amazon; (c, d) Central Africa; and (e, f) Southeast Asia. The dotted regions indicate regions covered by broadleaf evergreen trees in SSiB2.

The observed and simulated surface albedo is shown in Figure 8a. Although the surface albedo in the control SACOL run and GRTS SACOL run are both higher than the observed albedo, but the albedo in the GRTS run is consistently closer to the observation than that from the control SACOL run. Subsequently, the upward shortwave radiation in GTRS SACOL run is also more consistent with the observation data than that in the control SACOL run (Figure 8b).

5.2. Two-Dimensional Offline Model Evaluation

The single-point land surface model coupled with GRTS has shown the improvements of simulating the surface albedo and upward shortwave radiation. To test the GRTS application in two dimension regions, we ran the 2-D offline Simplified Simple Biosphere version 2 (SSiB2) land surface model coupled with GRTS. The model is driven by the Princeton University Hydroclimatology Group Bias Corrected Meteorological Forcing Dataset [*Sheffield et al*., 2006] at a resolution of 1.0° × 1.0°.

The control run is conducted using the two-stream method, and the sensitivity run using the GRTS is referred to as the GRTS run. Both experiments cover the period from 2000 to 2012. The first year is taken as a spin-up time, and the results of the last 12 years are analyzed below. According to the forest leaf angle observations

Table 3. Seasonal Bias of Land Surface Albedo Averaged for the Three Regions

	Amazon		Central Africa		Southeast Asia	
	CTL	GRTS	CTL	GRTS	CTL	GRTS
Winter	0.03	0.02	0.04	0.03	0.05	0.04
Spring	0.03	0.00	0.04	0.01	0.06	0.02
Summer	0.03	0.02	0.03	0.01	0.05	0.04
Autumn	0.03	0.00	0.03	0.00	0.05	0.02

[*Wang and Wang*, 1999], we use a nonuniform canopy structure, and the average leaf angles are 40° in the upper canopy layer, 20° in the middle, and 10° in the lower layers in broadleaf evergreen regions.

Differences in surface albedo between the GRTS run and the control run in Amazon, central Africa, and Southeast Asian, where the broadleaf evergreen trees cover most areas, are shown in Figure 9. The surface albedo in the control run is higher than MODIS surface albedo over most of these regions. The broadleaf evergreen regions have a nonuniform canopy structure with high LAI during the entire year, and the control run produces a relatively larger albedo. And this error may be caused by the nonuniform leaf angle distribution (LAD), which is not considered in the two-stream method. The error of the surface albedo in the GRTS run is smaller than that in the control run over most of broadleaf evergreen regions. The result from GRTS run is very close to the MODIS satellite data, and the error is generally less than 0.01. Table 3 shows the seasonal bias of surface albedo over Amazon, Central Africa and Southeast Asia. The GRTS run has better simulations in the spring and autumn than in the winter and summer. Moreover, the bias reveals that the surface albedo in GRTS run is more consistent with the satellite data than that in the control run with the two-stream method in the broadleaf evergreen regions. Similar to the bias results, the root-mean-square errors (table is not shown) reveal that the surface albedo in GRTS run is better than that in the control run with the two-stream method.

All sky albedo of MODIS composes of four parts: BSA_NIR, WSA_NIR, BSA_VIS, and WSA_VIS; the same as the land surface model. Figure 10 shows the simulated four bands of albedo and the MODIS products. In the control run, the simulated four bands of albedo are higher than MODIS products over most of the regions in the figure, especially for the BSA_NIR and WSA_NIR. The GRTS improves the performance of the BSA_NIR, WSA_NIR, and WSA_VIS albedo simulation, which are more noticeable in NIR domain. Only for the BSA_VIS the simulation becomes slightly worse in some areas.

The surface albedo would affect the surface energy balance. We compare the 12 year mean differences in canopy-absorbed and ground-absorbed radiation fluxes in Amazon, central Africa, and Southeast Asia (Figure 11) between the control run and the GRTS run. Most of broadleaf evergreen regions show a decrease in canopy absorption and an increase in ground absorption in the GRTS run compared to that in the control run. The canopy absorption usually changes in the opposite direction to changes in the ground absorption. The statistical results of the regional mean values for each season are shown in Table 4. The canopy-absorbed radiation flux shows lower values throughout the year in these three regions. The largest difference of $-18.4\,\mathrm{W\,m^{-2}}$ occurs in the Amazon region in the autumn. The ground-absorbed radiation flux increases throughout the year, especially in the spring and autumn. All the differences are larger than $13\,\mathrm{W\,m^{-2}}$, and the largest difference is $25.45\,\mathrm{W\,m^{-2}}$.

We assume that R is the downward radiation, R_a is the canopy reflected radiation, R_c is the canopy absorption, R_g is the ground absorption, R_t is the canopy transmission, and ρ_s is the soil reflectance:

$$R = R_a + R_c + R_g, \tag{28}$$

$$R_g = R_t \times (1 - \rho_s). \tag{29}$$

From the analysis in section 4.2, we know that the nonuniform LAD has a lower canopy reflectance and a higher transmittance. Thus, GRTS run has a lower albedo than that in the control run. The GRTS run has higher canopy transmission and thus higher ground absorption according to (29). Despite the decrease in the canopy reflected radiation and the increase in the ground absorption in the GRTS run, the magnitude of increase in the canopy reflected radiation is small. As a result, the canopy absorption is higher in the control run than that in the GRTS run.

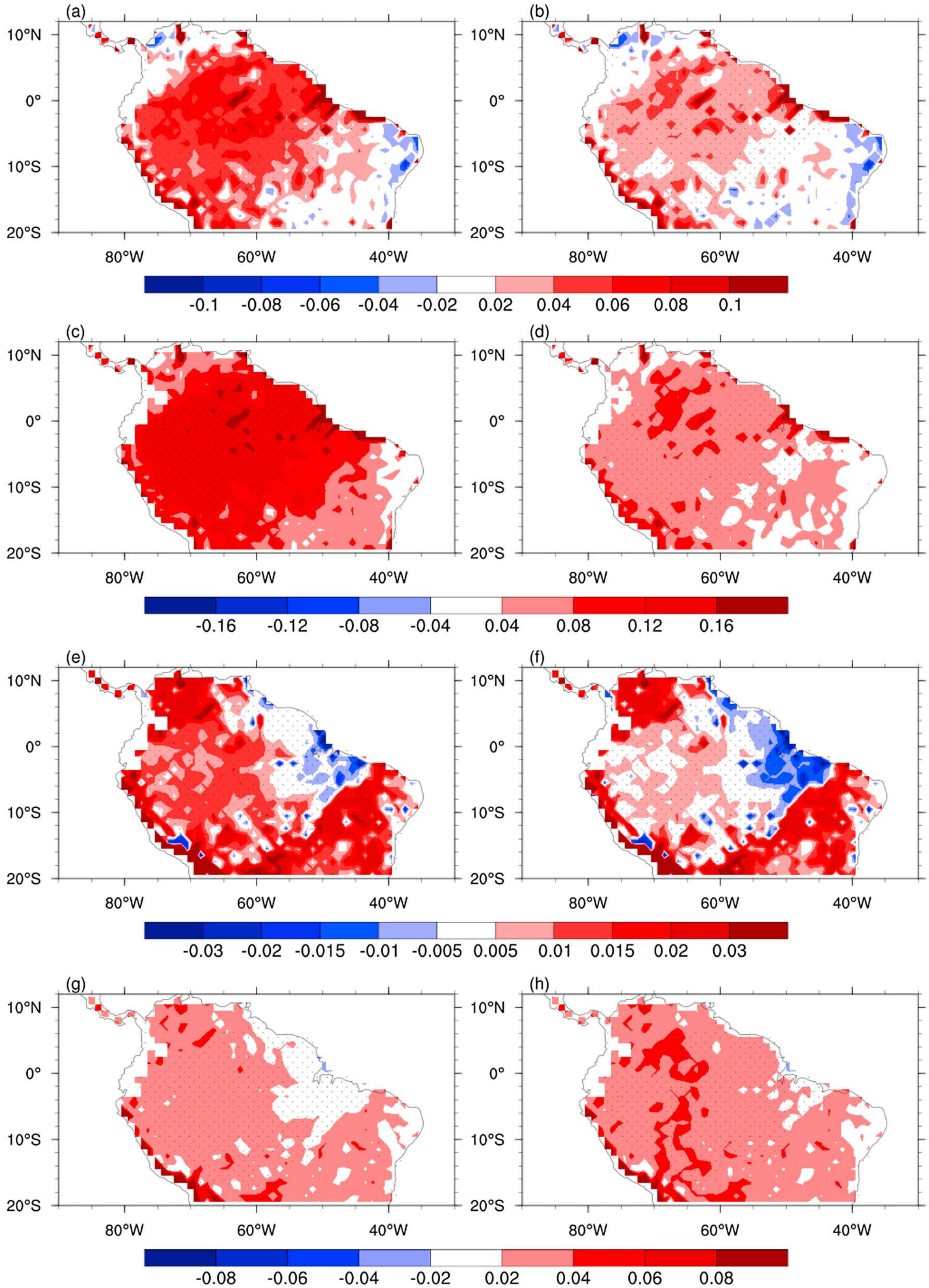

Figure 10. Annual mean error of land surface albedo in simulations of (a, c, e, and g) control run and (b, d, f, and h) GRTS run: (Figures 10a and 10b) WSA_NIR, (Figures 10c and 10d) BSA_ NIR, (Figures 10e and 10f) WSA_VIS, and (Figures 10g and 10h) BSA_VIS. The dotted regions indicate regions covered by broadleaf evergreen trees in SSiB2.

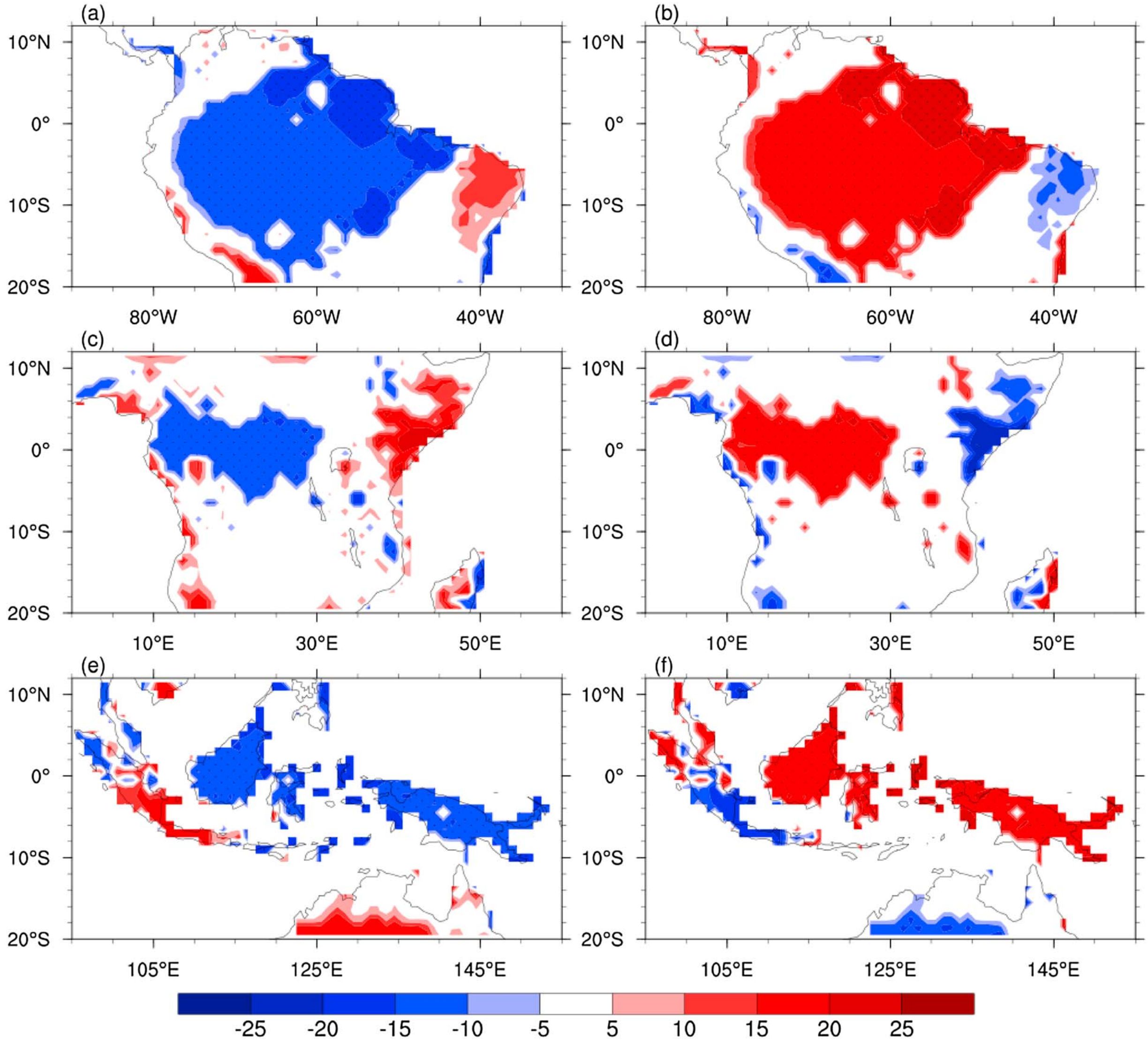

Figure 11. Annual mean differences in surface radiation fluxes (GRTS run minus control run). (a, b) Amazon; (c, d) Central Africa; and (e, f) Southeast Asia. (Figures 11a, 11c, and 11e) Canopy-absorbed radiation flux and (Figures 11b, 11d, and 11f) ground-absorbed radiation flux. Dotted regions indicate regions covered by broadleaf evergreen trees. Unit: W m^{-2}.

During the winter season when there is snow on the leaf surface, the reflectance of the adaxial leaf surface increases greatly, but the reflectance of the abaxial surface changes little with or without snow cover. The adaxial and abaxial optical differences should be included in the radiative transfer model under conditions of snow cover. But the difference between adaxial and abaxial optical properties is not distinguished in

Table 4. Seasonal Differences (GRTS Run Minus Control Run) in Surface Radiation Fluxes Averaged Over the Three Regions[a]

	Canopy-Absorbed Radiation Flux			Ground-Absorbed Radiation Flux		
	Amazon	Central Africa	Southeast Asia	Amazon	Central Africa	Southeast Asia
Winter	−11.67	−13.05	−13.26	14.35	16.16	16.22
Spring	−15.07	−17.20	−17.52	21.57	24.08	24.56
Summer	−12.08	−10.44	−10.90	15.07	13.11	13.57
Autumn	−18.40	−15.21	−18.37	25.33	21.49	25.45

[a]Units for radiation fluxes are W m^{-2}.

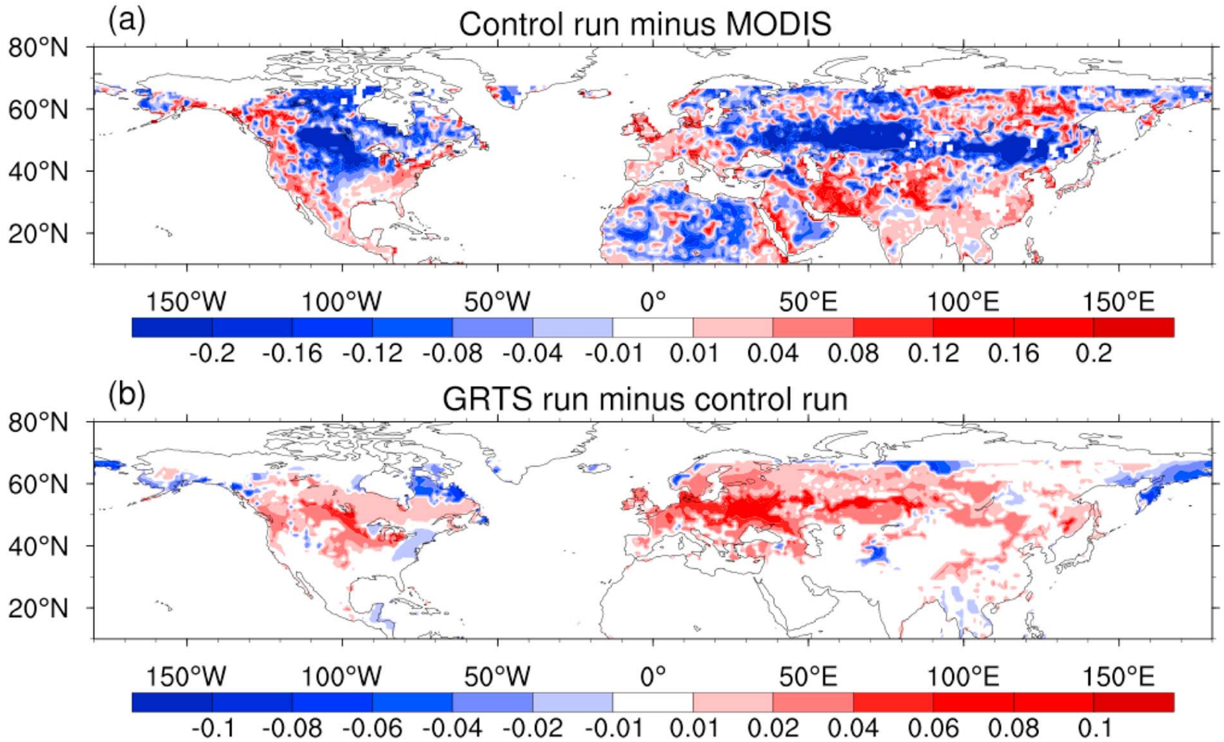

Figure 12. Mean differences in land surface albedo in the winter (DJF): (a) control run minus MODIS and (b) GRTS run minus control run.

the two-stream method. The GRTS takes into account the difference between adaxial and abaxial leaf optical properties as shown in Figure 2.

We compare the surface albedo using the averages of 12 year boreal winter (December, January, and February) mean results. The differences between the GRTS run and the control run in the Northern Hemisphere are shown in Figure 12. The surface albedo from the control run is smaller than MODIS surface albedo over most regions in the boreal winter. The region within latitudes 40–60°N shows a big negative bias of albedo compared to that from the MODIS data, and the difference is about −0.24 in some areas. The control run has a larger negative albedo bias in these areas mainly because the two-stream model cannot capture the high albedo value caused by snow cover in the dominant canopy in the winter. The previous studies also show that climate models have a large bias in simulating surface albedo in the region with snow cover [*Wang et al.*, 2006; *Brovkin et al.*, 2013]. The surface albedo from the GRTS run is larger than that from the control run over most of the boreal region. Central North America and most of central Europe show an increase in surface albedo in the GRTS run compared with that in the control run. Some of the large surface albedo differences between the control run and the GRTS run appear to be correlated with high snow cover fraction over the leaf in the model. Since the abaxial leaf in the GRTS has a lower albedo (no snow cover is considered), more reflected radiation from the ground would be transmitted upward and enhance the total canopy albedo. Figure 13 shows the differences in canopy-absorbed and ground-absorbed radiation fluxes in the winter from 2001 to 2012. Most of central Europe, East Asian, and India show a decrease in canopy absorption of about 10 $W\,m^{-2}$ and an increase in ground absorption of about 8 $W\,m^{-2}$ in the GRTS run compared with that in the control run. Central Asian and central western United States have an increase in canopy absorption of about 6 $W\,m^{-2}$ and a decrease in ground absorption of about 4 $W\,m^{-2}$.

6. Discussion and Conclusions

The two-stream radiative transfer model, which is widely used in current land surface models, is unrealistic in their assumptions of the same optical properties of adaxial and abaxial leaf surfaces and uniform LAD within the canopy. To have a more accurate description of the radiative transfer process, the GRTS parameterization

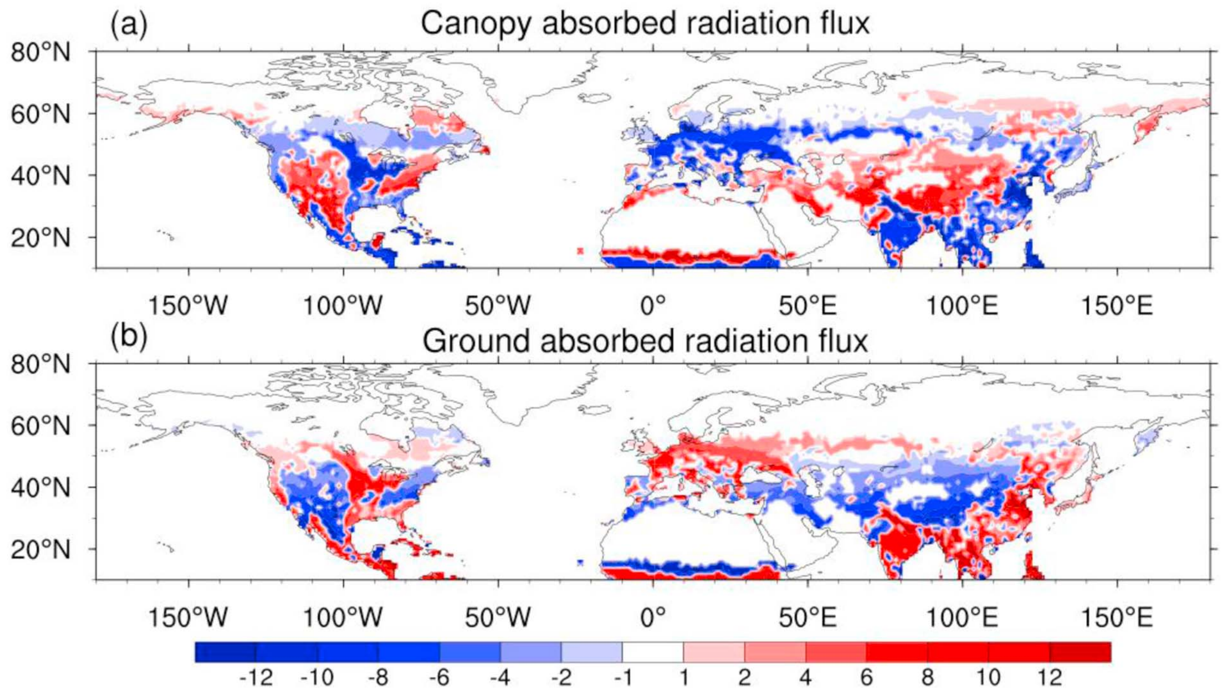

Figure 13. Mean differences in surface radiation fluxes in the winter (DJF) (GRTS run minus control run). (a) Canopy-absorbed radiation flux and (b) ground-absorbed radiation flux; unit: W m^{-2}.

has been developed. This model can be used in more general cases: nonuniform optical properties of adaxial and abaxial leaf surfaces and the nonuniform canopy structure in the vertical direction. The assumptions of the new scheme are expected to be more general and closer to reality. Sensitivity studies suggest that the nonuniform leaf angle distribution and leaf optical properties should be taken into account in the radiative transfer scheme. We coupled GRTS into the SSiB2 land surface model and compared it with the default two-stream model. This is a prototype study to implement GRTS in SSiB. This coupling approach, however, can be applied to any other land models.

The simulation of surface albedo in GRTS, which has nonuniform leaf angle distribution in the broadleaf evergreen trees areas, is better than that in the two-steam model. The canopy-absorbed radiation flux shows lower values throughout the year in the broadleaf evergreen trees areas. The biggest difference is -18.4 W/m^2 in the Amazon region in the autumn. The ground-absorbed radiation flux increases throughout the year, especially in the spring and autumn.

In the boreal wintertime, the large surface albedo differences between the control run and the GRTS run appear to be correlated with high snow cover fraction over leaf. And the GRTS has a better performance of simulating surface albedo in these areas. The partition between canopy absorption and ground absorption has been changed in the GRTS compared with the two-stream method. With more details information in comprehensive observational data, we will be able to further evaluate the model performance in these aspects and improve the model parameterization.

The vegetation and soil parameters (e.g., LAI, the fraction of greenness, leaf optical properties, and soil reflectance) in the land surface model have a profound impact on the simulations of surface albedo, canopy absorption, and ground absorption. Accurate representations of the plant function type and vegetation parameters are needed in the land surface model [*Qu and Hall*, 2014; *Wang et al*., 2016; *Liu et al*., 2016]. We will improve the vegetation distribution in the model based on satellite products. In addition, the soil albedo is a very important parameter in the simulation of the total surface albedo, especially in areas with small LAI. The observational MODIS data also show the dependence of soil albedo on the zenith angle [*Wang et al*., 2004]. However, the soil albedo represented in the current SSiB land surface model is the mean value of each soil type, which is independent of the zenith angle. This affects the simulation of surface albedo. Soil albedo will be adjusted through a fitting with the MODIS albedo data [*Lawrence and Chase*, 2007] in order to get a better match in the future. Nevertheless, GRTS is one step forward to provide a more realistic description of radiative transfer process within the canopy for use in climate modeling studies.

Acknowledgments
This work is jointly supported by the NSF of China grant (D0507/41475063 and D0512/91544231), U.S. NSF grant AGS-1419526, the National Science and Technology Support Program (2014BAC22B04), and Program for New Century Excellent Talents in University. This work is also supported by the Jiangsu Collaborative Innovation Center for Climate Change. The MODIS albedo products are processed and available at NASA Land Processes Distributed Active Archive Center (LP DAAC). The NCEP reanalysis climatology data are provided by the National Oceanic and Atmospheric Administration's (NOAA) Earth System Research Laboratory (ESRL) Physical Sciences Division (PSD). The model forcing data are available at http://hydrology.princeton.edu/data/pgf/1.0deg/3hourly/. We are grateful for the excellent supports provided by the people at SACOL, Lanzhou University. Sincere thanks go to the three anonymous reviewers for their insightful comments and suggestions which further improve the quality of the manuscript.

References

Brovkin, V., L. Boysen, T. Raddatz, V. Gayler, A. Loew, and M. Claussen (2013), Evaluation of vegetation cover and land-surface albedo in MPI-ESM CMIP5 simulations, *J. Adv. Model. Earth Syst.*, *5*, 48–57, doi:10.1029/2012MS000169.

Cescatti, A., et al. (2012), Intercomparison of MODIS albedo retrievals and in situ measurements across the global FLUXNET network, *Remote Sens. Environ.*, *121*, 323–334, doi:10.1016/j.rse.2012.02.019.

Charney, J., W. J. Quirk, S. H. Chow, and J. Kornfield (1977), Comparative study of effects of albedo change on drought in semi-arid regions, *J. Atmos. Sci.*, *34*, 1366–1385, doi:10.1175/1520-0469(1977)034<1366:ACSOTE>2.0.CO;2.

Chou, S. C., C. A. S. Tanajura, Y. Xue, and C. A. Nobre (2002), Validation of the coupled Eta/SSiB model over South America, *J. Geophys. Res.*, *107*(D20), 8088, doi:10.1029/2000JD000270.

Dai, Q., and S. Sun (2006), A generalized layered radiative transfer model in the vegetation canopy, *Adv. Atmos. Sci.*, *23*, 243–257, doi:10.1007/s00376-006-0243-7.

Dai, Q., and S. Sun (2007), A comparison of two canopy radiative models in land surface processes, *Adv. Atmos. Sci.*, *24*, 421–434, doi:10.1007/s00376-007-0421-2.

Dai, Y., and Q. Zeng (1997), A land surface model (IAP94) for climate studies. Part I: Formulation and validation in off-line experiments, *Adv. Atmos. Sci.*, *14*, 433–460, doi:10.1007/s00376-997-0063-4.

Dickinson, R. E. (1983), Land surface processes and climate—Surface albedos and energy balance, *Adv. Geophys.*, *25*, 305–353, doi:10.1016/S0065-2687(08)60176-4.

Dickinson, R. E., A. Henderson-Sellers, P. J. Kennedy, and M. F. Wilson (1986), Biosphere Atmosphere Transfer Scheme (BATS) for the NCAR Community Climate Model. *NCAR Tech. Note*, *NCAR*, *TN275+STR*, 69 pp.

Dirmeyer, P. A., and J. Shukla (1996), The effect on regional and global climate of expansion of the world's deserts, *Q. J. R. Meteorol. Soc.*, *122*, 451–482, doi:10.1002/qj.49712253008.

Gao, F., C. B. Schaaf, A. H. Strahler, A. Roesch, W. Lucht, and R. Dickinson (2005), MODIS bidirectional reflectance distribution function and albedo Climate Modeling Grid products and the variability of albedo for major global vegetation types, *J. Geophys. Res.*, *110*, D01104, doi:10.1029/2004JD005190.

Goudriaan, J. (1977), *Crop Micrometeorology: A Simulation Study*, Wageningen Univ, Wageningen, Netherlands.

Gu, L., D. D. Baldocchi, S. B. Verma, T. A. Black, T. Vesala, E. M. Falge, and P. R. Dowty (2002), Advantages of diffuse radiation for terrestrial ecosystem productivity, *J. Geophys. Res.*, *107*(D6), 4050, doi:10.1029/2001JD001242.

He, T., S. Liang, D. Wang, H. Wu, Y. Yu, and J. Wang (2012), Estimation of surface albedo and directional reflectance from Moderate Resolution Imaging Spectroradiometer (MODIS) observations, *Remote Sens. Environ.*, *119*, 286–300, doi:10.1016/j.rse.2012.01.004.

He, T., S. Liang, and D. Song (2014), Analysis of global land surface albedo climatology and spatial-temporal variation during 1981–2010 from multiple satellite products, *J. Geophys. Res. Atmos.*, *119*, 10,281–10,298, doi:10.1002/2014JD021667.

Huang, J.-P., et al. (2008), An overview of the semi-arid climate and environment research observatory over the Loess Plateau, *Adv. Atmos. Sci.*, *25*, 906–921, doi:10.1007/s00376-008-0906-7.

Jiang, Y. (1996), *A Study of the Structure and Function of Forest Ecosystems in China*, China Forestry Publishing House, Beijing.

Kalnay, E., M. Kanamitsu, R. Kistler, W. Collins, D. Deaven, L. Gandin, M. Iredell, S. Saha, G. White, and J. Woollen (1996), The NCEP/NCAR 40-year reanalysis project, *Bull. Am. Meteorol. Soc.*, *77*, 437–471, doi:10.1175/1520-0477(1996)077<0437:TNYRP>2.0.CO;2.

Lawrence, P. J., and T. N. Chase (2007), Representing a new MODIS consistent land surface in the Community Land Model (CLM 3.0), *J. Geophys. Res.*, *112*, G01023, doi:10.1029/2006JG000168.

Li, Q., S. Sun, and Y. Xue (2010), Analyses and development of a hierarchy of frozen soil models for cold region study, *J. Geophys. Res.*, *115*, D03107, doi:10.1029/2009JD012530.

Li, W., W. Guo, Y. Xue, C. Fu, and B. Qiu (2015), Sensitivity of a regional climate model to land surface parameterization schemes for East Asian summer monsoon simulation, *Clim. Dyn.*, 1–16, doi:10.1007/s00382-015-2964-8.

Liang, S. (2004), *Quantitative Remote Sensing of Land Surfaces*, John Wiley, Hoboken, N. J.

Liu, Y., W. Guo, and Y. Song (2016), Estimation of key surface parameters in semi-arid region and their impacts on improvement of surface fluxes simulation, *Sci. China Earth Sci.*, *59*, 307–319, doi:10.1007/s11430-015-5140-4.

Loranty, M. M., L. T. Berner, S. J. Goetz, Y. Jin, and J. T. Randerson (2014), Vegetation controls on northern high latitude snow-albedo feedback: Observations and CMIP5 model simulations, *Global Change Biol.*, *20*, 594–606, doi:10.1111/gcb.12391.

Lucht, W., C. B. Schaaf, and A. H. Strahler (2000), An algorithm for the retrieval of albedo from space using semiempirical BRDF models, *IEEE Trans. Geosci. Remote Sens.*, *38*, 977–998, doi:10.1109/36.841980.

Meador, W. E., and W. R. Weaver (1980), Two-stream approximations to radiative transfer in planetary atmospheres: A unified description of existing methods and a new improvement, *J. Atmos. Sci.*, *37*, 630–643, doi:10.1175/1520-0469(1980)037<0630:TSATRT>2.0.CO;2.

Mesarch, M. A., E. A. Walter-Shea, and C. J. Hays (1998), BOREAS TE-12 leaf optical data for SSA species Data set. Available on-line [http://www.daac.ornl.gov] from Oak Ridge National Laboratory Distributed Active Archive Center, Oak Ridge, Tenn, doi:10.3334/ORNLDAAC/352.

Myneni, R., V. Gutschick, G. Asrar, and E. Kanemasu (1988), Photon transport in vegetation canopies with anisotropic scattering: Part II. Discrete-ordinates/exact-kernel technique for one-angle photon transport in slab geometry, *J. Agric. For. Meteorol.*, *42*, 17–40, doi:10.1016/0168-1923(88)90064-0.

Niu, G. Y., et al. (2011), The community Noah land surface model with multiparameterization options (Noah-MP): 1. Model description and evaluation with local-scale measurements, *J. Geophys. Res.*, *116*, D12109, doi:10.1029/2010JD015139.

Norman, J. M., and P. G. Jarvis (1975), Photosynthesis in Sitka spruce (Picea sitchensis (Bong.) Carr.): V. Radiation penetration theory and a test case, *J. Appl. Ecol.*, *12*, 839–878, doi:10.2307/2402094.

Oleson, K. W., G. B. Bonan, C. Schaaf, F. Gao, Y. Jin, and A. Strahler (2003), Assessment of global climate model land surface albedo using MODIS data, *Geophy. Res. Lett.*, *30*(8), 1443, doi:10.1029/2002GL016749.

Qu, X., and A. Hall (2014), On the persistent spread in snow-albedo feedback, *Clim. Dyn.*, *42*, 69–81, doi:10.1002/2015JD023824.

Schaaf, C. B., et al. (2002), First operational BRDF, albedo nadir reflectance products from MODIS, *Remote Sens. Environ.*, *83*, 135–148, doi:10.1016/S0304-3800(99)00180-5.

Sellers, P. J. (1985), Canopy reflectance, photosynthesis and transpiration, *Int. J. Remote Sens.*, *6*, 1335–1372, doi:10.1080/01431168508948283.

Sellers, P. J., Y. Mintz, Y. C. Sud, and A. Dalcher (1986), A simple biosphere model (SiB) for use within general circulation models, *J. Atmos. Sci.*, *43*, 505–531, doi:10.1175/1520-0469(1986)043<0505:ASBMFU>2.0.CO;2.

Sellers, P. J., D. A. Randall, G. J. Collatz, J. A. Berry, C. B. Field, D. A. Dazlich, C. Zhang, G. D. Collelo, and L. Bounoua (1996), A revised land surface parameterization (SiB2) for atmospheric GCMS. Part I: Model formulation, *J. Clim.*, *9*, 676–705, doi:10.1175/1520-0442(1996)009<0676:ARLSPF>2.0.CO;2.

Sheffield, J., G. Goteti, and E. F. Wood (2006), Development of a 50-year high-resolution global dataset of meteorological forcings for land surface modeling, *J. Clim.*, *19*, 3088–3111, doi:10.1175/JCLI3790.1.

Stroeve, J., J. E. Box, F. Gao, S. Liang, A. Nolin, and C. Schaaf (2005), Accuracy assessment of the MODIS 16-day albedo product for snow: Comparisons with Greenland in situ measurements, *Remote Sens. Environ.*, *94*, 46–60, doi:10.1016/j.rse.2004.09.001.

Sud, Y. C., and M. Fennessy (1982), A study of the influence of surface albedo on July circulation in semi-arid regions using the GLAS GCM, *J. Climatol.*, *2*, 105–125, doi:10.1002/joc.3370020202.

Sun, S., and Y. Xue (2001), Implementing a new snow scheme in Simplified Simple Biosphere Model (SSiB), *Adv. Atmos. Sci.*, *18*, 335–354, doi:10.1007/BF02919314.

Tian, Y., R. E. Dickinson, and L. Zhou (2007), Four-stream isosector approximation for canopy radiative transfer, *J. Geophys. Res.*, *112*, D04107, doi:10.1029/2006JD007545.

Wang, H., and X. Wang (1999), *Principles and Techniques on the Biological Boundary Layer*, China Meteorological Press, Beijing.

Wang, L., J. N. S. Cole, P. Bartlett, D. Verseghy, C. Derksen, R. Brown, and K. von Salzen (2016), Investigating the spread in surface albedo for snow-covered forests in CMIP5 models, *J. Geophys. Res. Atmos.*, *121*, 1104–1119, doi:10.1002/2015JD023824.

Wang, S., A. P. Trishchenko, K. V. Khlopenkov, and A. Davidson (2006), Comparison of international panel on climate change fourth assessment report climate model simulations of surface albedo with satellite products over northern latitudes, *J. Geophys. Res.*, *111*, D21108, doi:10.1029/2005JD006728.

Wang, S., A. P. Trishchenko, and X. Sun (2007), Simulation of canopy radiation transfer and surface albedo in the EALCO model, *Clim. Dyn.*, *29*, 615–632, doi:10.1007/s00382-007-0252-y.

Wang, Z., X. Zeng, M. Barlage, R. E. Dickinson, F. Gao, and C. Schaaf (2004), Using MODIS BRDF and albedo data to evaluate global model land surface albedo, *J. Hydrometeorol.*, *5*, 3–14, doi:10.1175/1525-7541(2004)005<0003:UMBAAD>2.0.CO;2.

Wohlfahrt, G., M. Bahn, U. Tappeiner, and A. Cernusca (2000), A model of whole plant gas exchange for herbaceous species from mountain grassland sites differing in land use, *Ecol. Model.*, *125*, 173–201, doi:10.1016/S0304-3800(99)00180-5.

Xue, Y., and J. Shukla (1993), The influence of land surface properties on Sahel climate. Part 1: Desertification, *J. Clim.*, *6*, 2232–2245, doi:10.1175/1520-0442(1993)006<2232:TIOLSP>2.0.CO;2.

Xue, Y., P. J. Sellers, J. L. Kinter, and J. Shukla (1991), A simplified biosphere model for global climate studies, *J. Clim.*, *4*, 345–364, doi:10.1175/1520-0442(1991)004<0345:ASBMFG>2.0.CO;2.

Xue, Y., F. Zeng, and C. A. Schlosser (1996a), SSiB and its sensitivity to soil properties: A case study using HAPEX-Mobilhy data, *Global Planet. Change*, *13*, 183–194, doi:10.1016/0921-8181(95)00045-3.

Xue, Y., M. J. Fennessy, and P. J. Sellers (1996b), Impact of vegetation properties on U.S. summer weather prediction, *J. Geophys. Res.*, *101*, 7419–7430, doi:10.1029/95JD02169.

Xue, Y., S. Sun, D. S. Kahan, and Y. Jiao (2003), Impact of parameterizations in snow physics and interface processes on the simulation of snow cover and runoff at several cold region sites, *J. Geophys. Res.*, *108*(D22), 8859, doi:10.1029/2002JD003174.

Xue, Y., F. De Sales, R. Vasic, C. R. Mechoso, A. Arakawa, and S. Prince (2010), Global and seasonal assessment of interactions between climate and vegetation biophysical processes: A GCM study with different land-vegetation representations, *J. Clim.*, *23*, 1411–1433, doi:10.1175/2009JCLI3054.1.

Yang, R., M. A. Friedl, and W. Ni (2001), Parameterization of shortwave radiation fluxes for nonuniform vegetation canopies in land surface models, *J. Geophys. Res.*, *106*, 14,275–14,286, doi:10.1029/2001JD900180.

Yuan, H., R. E. Dickinson, Y. Dai, M. J. Shaikh, L. Zhou, S. Wei, and D. Ji (2014), A 3D canopy radiative transfer model for global climate modeling: Description, validation, and application, *J. Clim.*, *27*, 1168–1192, doi:10.1175/JCLI-D-13-00155.1.

Zhan, X., Y. Xue, and G. J. Collatz (2003), An analytical approach for estimating CO_2 and heat fluxes over the Amazonian region, *Ecol. Model.*, *162*, 97–117, doi:10.1016/S0304-3800(02)00405-2.

Zhang, X., S. Liang, K. Wang, L. Li, and S. Gui (2010), Analysis of global land surface shortwave broadband albedo from multiple data sources, *IEEE J. Sel. Top. Appl. Earth Obs. Remote Sens.*, *3*, 296–305, doi:10.1109/JSTARS.2010.2049342.